npj | climate and atmospheric science

www.nature.com/npjclimatsci

ARTICLE OPEN

Check for updates

Tracing the formation of exceptional fronts driving historical fires in Southeast Australia

Leehi Magaritz-Ronen[1]✉ and Shira Raveh-Rubin[1]

Extreme cold fronts are closely associated with the spread of large wildfires in Australia. The strength of a front is determined by the drop in temperature across it, which will in turn be determined by the warm and cold temperature anomalies on either side of the front. Here, we examine the Black Saturday and Ash Wednesday fires in southeast Australia through a Lagrangian decomposition framework, exploring the origin of the potential temperature anomalies that formed these extreme cold fronts. We identify the contributions of three processes: an initial anomaly at the origin, adiabatic transport of climatologically different air, and diabatic heating along the air-parcel trajectory. We find that on both sides of the cold front descending trajectories contribute to the extreme anomalies. In the warm sector, positive anomalies arrive with descending trajectories from the Indian Ocean. In the cold sector, negative anomalies are dominated by strongly descending dry intrusions forming as part of the cyclonic system. The dry intrusions advect colder air, overcompensating for its adiabatic warming during its descent. Identification of the precursors and the mechanisms contributing to extreme cold fronts associated with large wildfires can improve the forecast of such events and help evaluate them in future climate projections.

npj Climate and Atmospheric Science (2023)6:110 ; https://doi.org/10.1038/s41612-023-00425-z

INTRODUCTION

As wildfires endanger vast areas of vegetation, wildlife and human population, understanding the factors affecting the spread of fire is of great importance. Studies indicate that wildfires may increase in frequency and intensity in the near future under a warming climate with clear trends observed in several parts of the world, including western United States[1] and Australia[2]. In Southeast Australia an increase in fire weather frequency has been associated with a poleward shift of the storm track[3,4] and an increase in frequency of cold fronts has been associated with the Australian fire season of 2019-2020[5]. Historical extreme wildfires can provide insight into the conditions leading to the spread of such disastrous events. Understanding the precursors and contributing mechanisms can improve forecast and management of these events by incorporating and identifying them in weather prediction and fire management models and may increase forecast accuracy and enhance early warning systems. Furthermore, understanding the underlying mechanisms will help evaluate wildfire behavior under future climate scenarios.

Many components act together during wildfire outbreaks, and involve both land and atmospheric systems and feedbacks that produce the right environmental conditions. Considering atmospheric *systems* that govern the environmental *conditions*, cold fronts are the most prominent ones in southeast Australia. Cold fronts are formed within a synoptic environment of a large temperature gradient, and here it is our goal to understand its drivers. Atmospheric mechanisms of varying scales have been associated with the spread of these wildfires, from large scale phenomena such as Rossby wave breaking in the upper levels with a strong potential vorticity (PV) anomaly[6] to smaller, shorter-term weather phenomena such as a sharp temperature gradient on the 850 hPa level[7,8], or abrupt surface drying[9]. The spread of the largest fires in Southeast Australia is most commonly associated with the passage of extreme cold fronts[6,7,10–12]. Strong winds as well as changes in wind direction that accompany the passage of the front lead to a rapid growth of an extended fire progression line. The speed of the passing front at the surface is connected to the speed of the synoptic system in which it is embedded[13]. Such intense fronts are characterized by high temperature anomalies and extreme heat waves ahead of the front[11,14,15] and cold temperature anomalies behind it. In this study we focus on the large scale dynamical processes leading to the conditions surrounding the formation of the cold front.

A Lagrangian approach that tracks the evolution of temperature along the motion of the selected air masses[15–18] can be useful for understanding temperature anomalies. Because potential temperature is conserved in adiabatic processes, changes in the potential temperature along the trajectory allow us to isolate three factors that contribute to the anomaly θ' at the target time t_1 and location x_1. The anomaly is defined as the difference of potential temperature (θ) from its local climatological mean (θ_{clim}), as described in the equation:

$$\theta'(t_1,x_1) = \theta'(t_0,x_0) + (\theta(t_1,x_1) - \theta(t_0,x_0)) + (\theta_{clim}(t_0,x_0) - \theta_{clim}(t_1,x_1)) \quad (1a)$$

where the RHS of the equation represents the adiabatic advection of an initial anomaly that existed in the air mass origin (t_0, x_0), diabatic heating along the air mass trajectory resulting in changes to potential temperature of the air mass, and adiabatic transport of climatologically different air masses from the air mass origin, respectively. In this study we revisit two large historical wildfires, the Black Saturday fire of 2009 and the Ash Wednesday fire of 1983. We implement a Lagrangian framework and analyze air mass trajectories in each case, to examine the origin of the extreme temperature drop across the cold front. A decomposition method for the potential temperature anomaly is then used to identify the dynamical processes that led to the formation of the observed extreme anomalies in both cases.

[1]Department of Earth and Planetary Sciences, Weizmann Institute of Science, Rehovot, Israel. ✉email: leehi.magaritz-ronen@weizmann.ac.il

RESULTS

The Black Saturday fires

The record-breaking Black Saturday fires started on February 7, 2009. The fires consumed over 450,000 hectares of land and killed 173 people[11], making them one of the most devastating fires in southeast Australia's history. The weather pattern during these days was common fire weather for this region, characterized by two anticyclones in the Southern Ocean, with a surface low between them, resulting in a summertime frontogenesis region[10,11] (Fig. 1a, see also supplementary fig. 2). The region of the cold front can be seen by the white shading in the colormap in Fig. 1a, b. Uncommonly, the cyclone associated with the Black Saturday fires was one of the strongest on record, leading to dangerous fire conditions, with the cyclone's central sea level pressure (SLP) dropping to 980 hPa with high temperatures observed already in the days before the fire began[8,11]. In fact, before the cold front passed on 7 February at 6:00 UTC, the temperatures at Melbourne Airport reached a record-breaking 46.8 °C, as part of one of the most severe heatwaves observed in southeastern Australia[11,15,19]. Such extreme temperature had not been recorded even during the heatwave preceding the 2020 "Black Summer" fires[20]. With the cold front passage, the temperature dropped quickly in several locations by 15 °C[6,11], reaching below the lowermost 1 percentile threshold for February. This extreme front occurred under the last stages of a Rossby wave overturning (Fig. 1a), a feature frequently associated with extreme fire weather in Southeast Australia[6].

The change of the air masses during the passage of the cold front was examined by the backward trajectories at each time step, i.e. before and after the cold front (bottom panels in Fig. 1). The back trajectories were initiated from an area larger than the location of the front line in order to incorporate larger scale air flows affecting the area of the fires. Before the cold front (Fig. 1c), two distinct air streams, governed by easterly and westerly winds, converge into the target region. This flow pattern is a result of the two anticyclones located to the east and west of the cyclone south of the Australian continent. The easterly trajectories remain in the lower troposphere, close to the ocean or land surface, with limited vertical displacement. In contrast, the westerly trajectories (Fig. 1c) descend from the upper and middle troposphere to the west of the continent. These descending westerly trajectories that arrive into the warm sector are driven by the preceding anticyclone and upper level anticyclonic PV anomaly that contributed to the extreme heatwave in the area[14,15] (see also supplemental video 1) Although the origin and properties of these flows are very different, we show that they both led to a positive temperature anomaly in the warm sector of the cyclone.

Major wind shifts occurred with the passage of the cold front. On the cold side of the front the flow arrived from the south-southwest (Fig. 1d), comprised mainly of descending air streams that are part of a large dry intrusion[21,22] (DI), but it also included some low level winds arriving from the same direction. Most trajectories arrived from the upper troposphere above the coast of Antarctica, and descended towards the surface. Some trajectories descended more than 400 hPa in 48 h, conforming to the global Lagrangian criterion for DIs set in Raveh-Rubin (2017)[23]. Such DIs occur less than 1% of the time in southeast Australia in summer[23] demonstrating the rareness of this event.

For the calculated trajectories we used the decomposition method to identify the origin and processes contributing to the potential temperature anomaly. The potential temperature

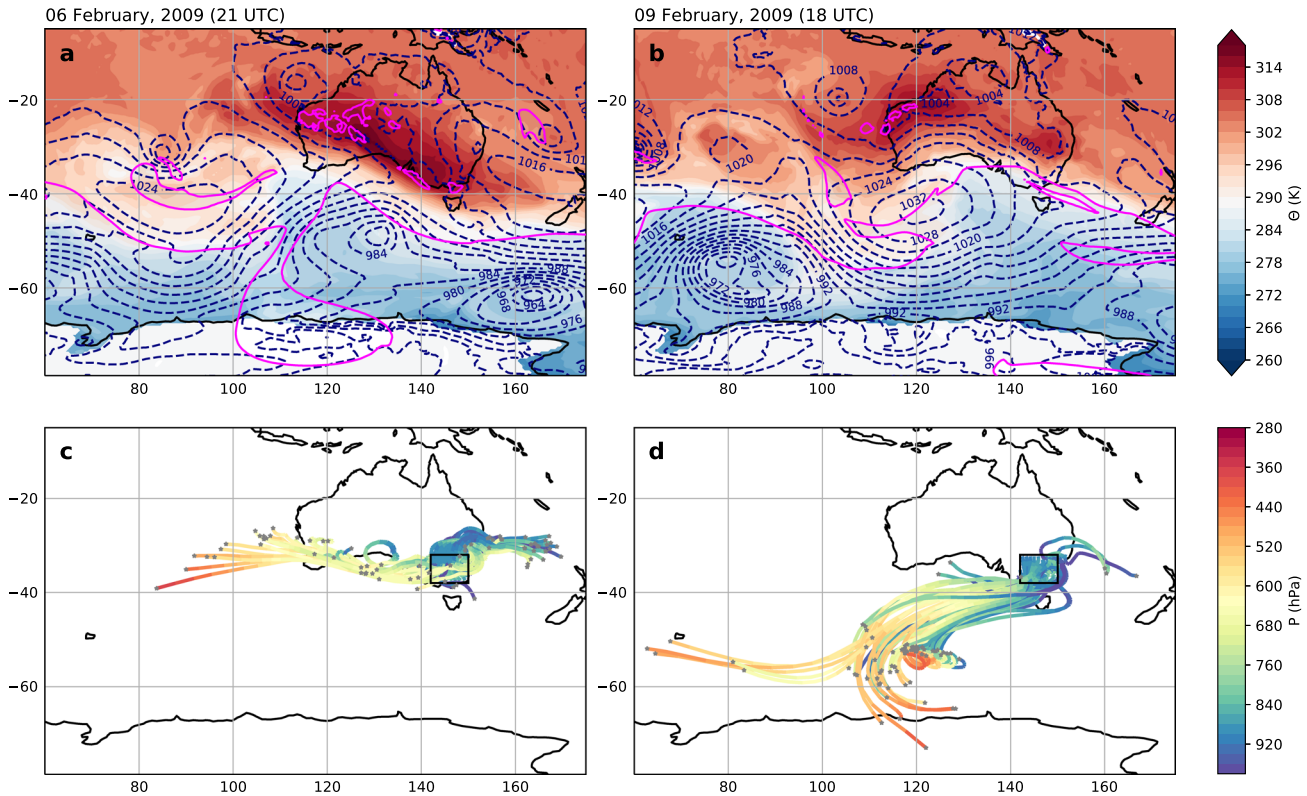

Fig. 1 Synoptic conditions and air mass trajectories before and after the cold front in the Black Saturday fires. Potential temperature on 850 hPa geopotential (shading, K), SLP (dashed contours, hPa) and the dynamical tropopause in magenta (−2 PVU on the 330-K isentrope, Hoskins[40]), before (**a**) and after (**b**) the passage of the cold front. Two examples of trajectories calculated backwards from the same dates, before (**c**) and after (**d**) the cold front. Trajectories are colored by pressure (hPa), gray markers represent the location of the air masses at −96 h. SLP is plotted for the start time of the back trajectory, when the trajectories arrive to the surface. The black box marks the area of the trajectories' starting positions.

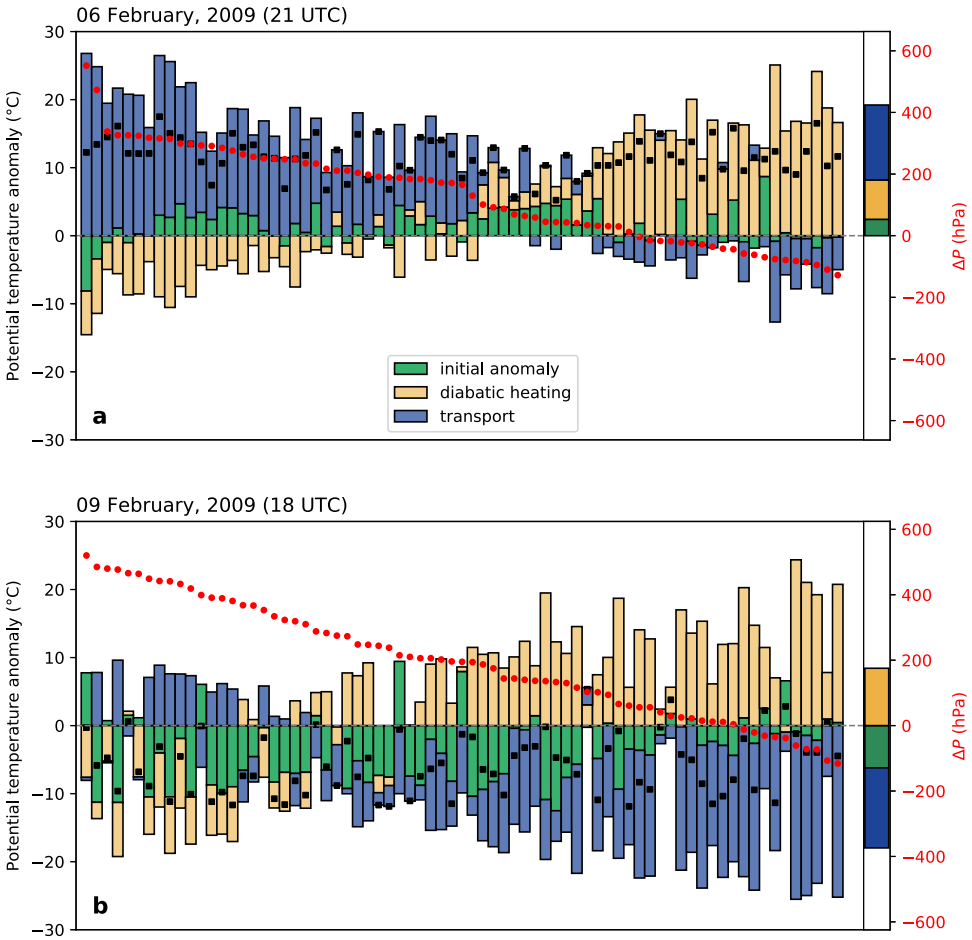

Fig. 2 Decomposition of θ' into its contributing terms in the Black Saturday fires. Two time steps are presented **a** before and **b** after the cold front (corresponding to Fig. 1). Each bar represents one calculated back-trajectory starting at the stated time, sorted by ΔP. The black markers represent target θ'. The right *y*-axis and the red markers represent ΔP of the trajectory, $P(0h) - P(-96h)$. The thicker bar on the right is the average contribution of all trajectories.

anomaly for each of the trajectories, $\theta'(t_1, x_1)$, is marked with a black marker in Fig. 2. The trajectories are sorted by the pressure difference along their path, with positive values indicating descent of the air mass (right axis Fig. 2). Each of the elements in Eq. 1a comprising θ' was calculated for the time interval of 0–96 h (i.e., $t_0 = -96\,h$) and plotted in Fig. 2 as bars centered around zero, to show positive and negative contributions.

As was first indicated by the trajectories themselves (Fig. 1c), two types of air masses arrived into the warm sector, both leading to a warm θ' (Fig. 2a). For trajectories with a small ΔP, positive or negative, the main contributing factor in the anomaly is diabatic heating, in which sensible and latent heat fluxes increase the potential temperature of air masses along near-surface easterlies (Fig. 1c). A close examination of these trajectories revels some of the small-scale features affecting the frontogenesis in the region such as subsidence of the air masses before the ascent in the warm conveyor belt or cross-frontal flow which is characterized by small scale ascent before the front[13]. It is interesting to note that for these subsiding air masses (small positive ΔP, middle part in Fig. 2a) there were equal contributions of an initial temperature anomaly and diabatic heating which both contribute to the overall positive temperature anomaly. Trajectories with negative ΔP and localized processes in the frontogenesis area require further investigation in future studies.

For descending westerlies, with large positive ΔP, the main contributing factor was the transport of climatologically different air masses. Diabatic processes were negative in these trajectories, and acted as a mitigating factor balancing the strong positive anomaly in those trajectories with large ΔP. Radiative cooling is the likely mechanism to cause these diabatic effects. It is important to note that although the origins and paths of the air masses are very different they all led to a positive θ'.

After the passage of the cold front, when the winds shift to southerlies, with most trajectories coming from the same direction (Fig. 1d), θ' is negative. Again, there were two main types of trajectories (Fig. 2b). Descending trajectories in the cold sector arrive from the south and from higher levels, with a ΔP of 400–600 hPa. Such extreme values indicate that these descending air streams constitute a DI that formed as part of the passing cyclonic system. The combination of an initial cold anomaly at the origin of the airflow with diabatic (likely radiative) cooling of descending trajectories leads to the cold anomaly at the target region. For trajectories with smaller ΔP there were different contributing factors, while the anomaly was still negative. Coming from the south, the air masses cross horizontal θ gradients and therefore transport climatologically colder air in the lower troposphere. However, the resulting anomaly was counterbalanced by diabatic heating, most likely due to surface fluxes, as the air mass moved towards warmer waters, resulting in cold anomalies comparable to those from the strongly-descending DIs.

Many small scale dynamical processes may affect the formation of the cold front, as demonstrated in the variability among the trajectories initiated in a single time step shown in Fig. 2. All these processes are incorporated into the investigation of the large scale

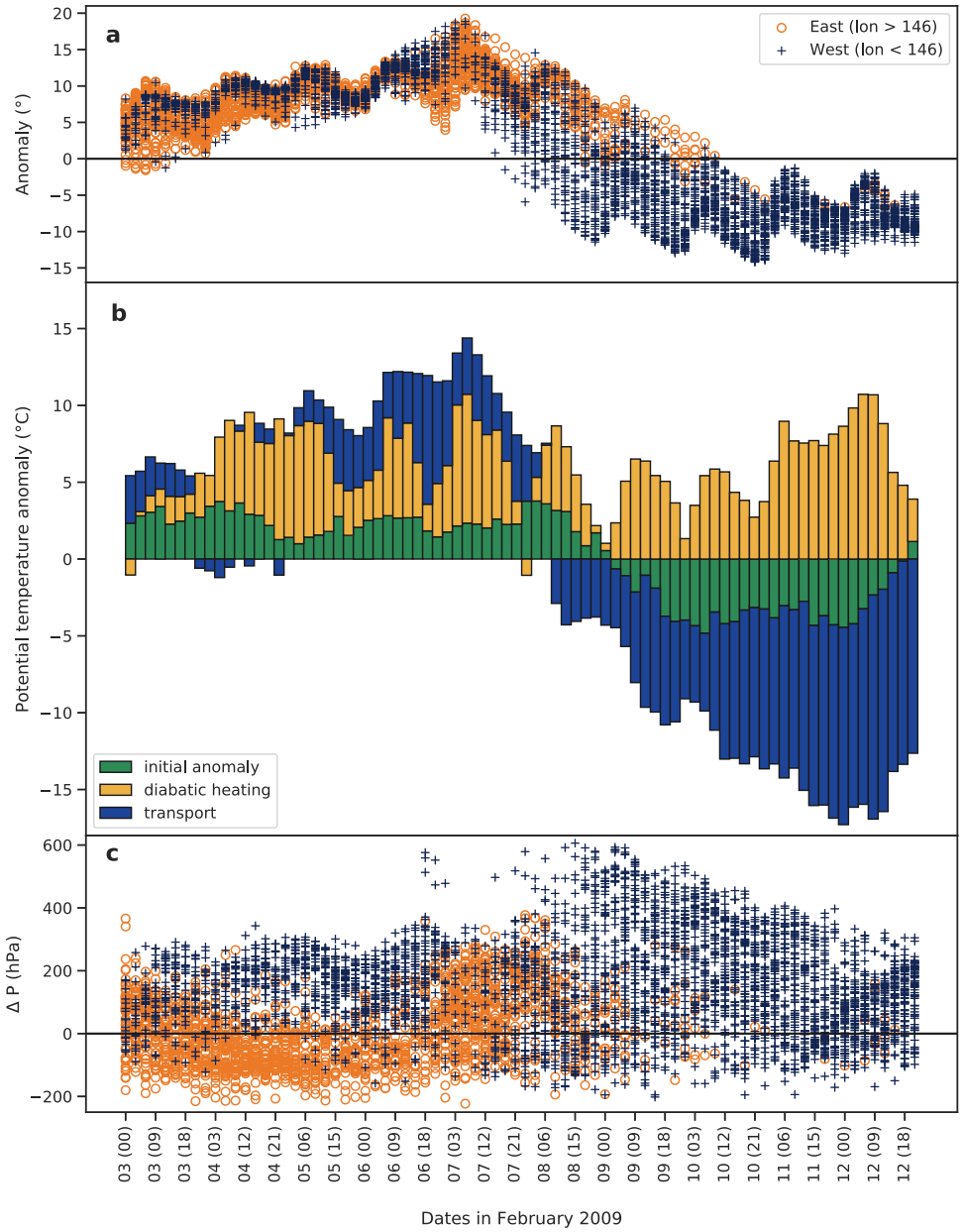

Fig. 3 Evolution of the contributing factors along the front in the Black Saturday fires. In the figure trajectories from every 3 h between February 3–12, 2009 (hours in UTC), showing (**a**) the target θ', each point represents one trajectory. Color indicates the origin of the trajectories, east or west of 146E longitude; (**b**) the θ' decomposition, each bar represents the average of the contributions in all trajectories starting at that time (compare to the mean bars on the right side in Fig. 2); and (**c**) ΔP of each trajectory, colors as in (**a**).

conditions leading to the formation of the cold front. To this end, we averaged the different contributions at each time step (side bar in Fig. 2) and looked at the evolution of these average contributions in time during the passage of the cold front (Fig. 3). Each bar in Fig. 3b represents the average of all positive and negative contributions from the different trajectories calculated from a single time step, while θ' and ΔP for each trajectory (colored by the origin longitude of the air mass) are shown in the upper and lower panels.

In the days prior to the passage of the cold front, the potential temperature anomaly was positive (Fig. 3a), with values increasing up to $+20°$. Positive θ' in the target area was a result of contributions from both east and west, due to different dynamical processes, with ΔP ranging from -200 hPa to about $+200$ hPa (Fig. 3c). And yet, all of these trajectories led to a positive θ', surprisingly of the same order. A close examination of the scatterplots shows that the westerly trajectories with the largest ΔP lead to the larger θ' values.

The decomposition analysis showed that the extreme positive temperature anomaly in the warm sector was a result of all three contributing factors: the transport of climatologically warmer air mass, a positive anomaly already at the origin, and diabatic heating. As shown in Fig. 2, the diabatic heating was mostly due to easterly low level trajectories heated by surface fluxes with a peak in the contribution during daytime (Fig. 3b). The transport and initial anomaly contributions were from the descending trajectories that arrived from the west (Fig. 3c). These air masses arrived from higher latitudes, advecting the climatological properties of their origin.

In the warm sector, when extreme temperature records were broken in the region, a pronounced contribution of a positive initial anomaly at the origin also seen. The origin of the warm

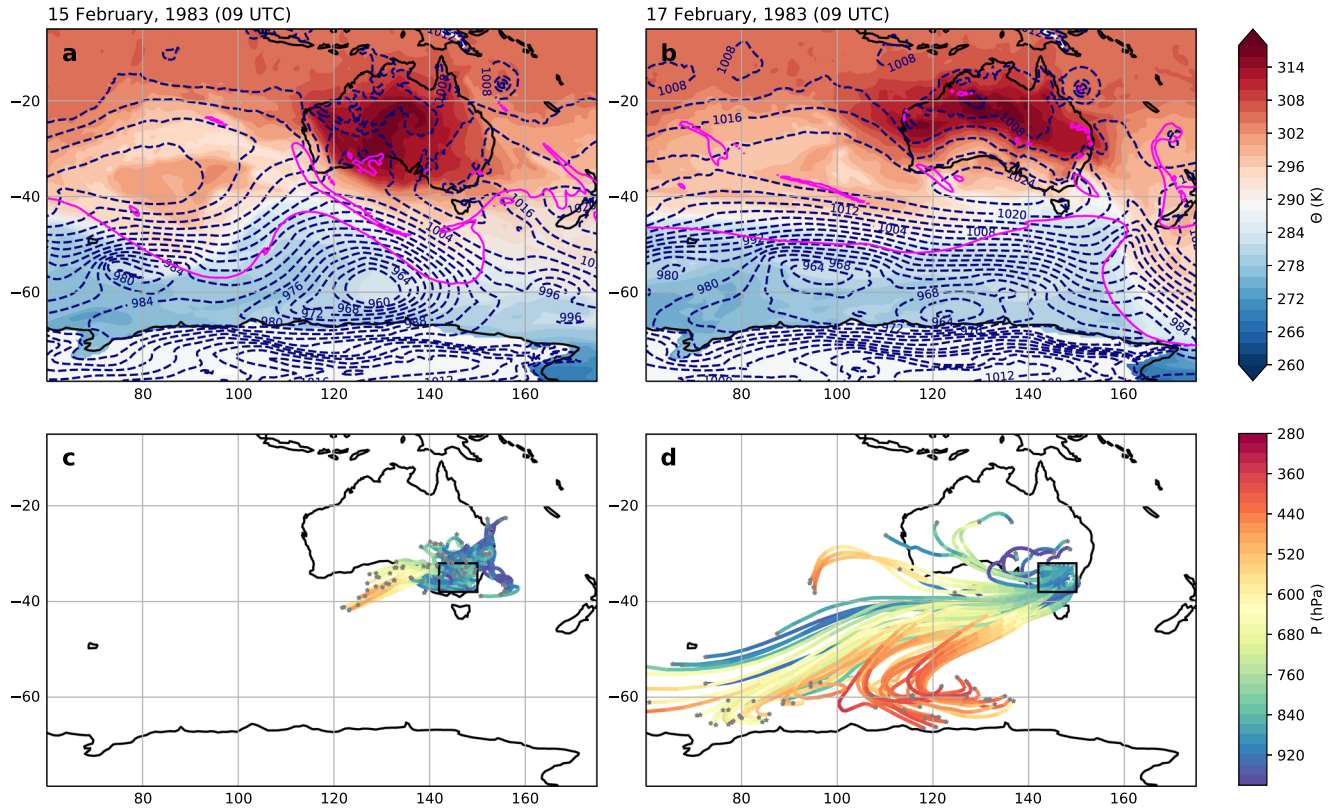

Fig. 4 Synoptic conditions and air mass trajectories before and after the Ash Wednesday fires. Potential temperature on 850 hPa geopotential (shading, K), SLP (dashed contours, hPa) and the dynamical tropopause in magenta (−2 PVU on the 330-K isentrope, Hoskins[40]), at representative dates before (**a**) and after (**b**) the passage of the cold front. Trajectories calculated backwards from the same dates, before (**c**) and after (**d**) the cold front. Trajectories are colored by pressure (hPa), gray markers represent the location of the air masses at −96 h. SLP is plotted for the start time of the back trajectory, when the trajectories arrive to the surface. The black box marks the area of the trajectories' starting positions.

anomaly is out of the scope of this paper, however, we note that air masses contributing to the extreme heat wave before Black Saturday and to heat waves in Southeast Australia in general were found to originate near tropical cyclones and to aggregate near southwestern Australia, before affecting extreme temperatures in Victoria[19]. Also, alternatively, heat waves in the region can be traced back to air masses previously heated while ascending over the western Indian Ocean and descending towards southeast Australia [15]. Both of these processes can lead to the initial anomaly found in the decomposition results (Fig. 3b).

The cold front passed Melbourne in the afternoon of February 7 (local time, UTC + 11) and is seen in Fig. 3 by a decrease in θ' in all trajectories (Fig. 3a). Since we considered an average across an area (box in Fig. 1) rather than a single point, it appears that it takes the cold front 24 h to pass, this is in fact the time it takes the cold front to pass through the entire selected area. During these time steps, we are able to see the warm anomalies from the warm sector and the cold anomalies after the cold front simultaneously. Amazingly, these anomalies spanned over 20 °C, from +15 to −10, leading to the formation of the extreme cold front.

Behind the cold front two air streams originated in the southwest, a lower level flow and a DI arriving from the upper levels, both introduced negative θ'. As the cold front progressed, the climatological "transport" contribution increased, meaning that air that is climatologically colder by 5–15 °C is advected into the target region. The large negative transport contribution was a result of the low-level flow crossing the climatological gradient of θ, as shown in Fig. 2b. After the front, the contribution of the negative initial anomaly from the descending DI trajectories increased. These air masses with the largest ΔP have the coldest anomalies coming into the region (Fig. 3c). The resulting extreme cold anomaly from the combined air streams were maximal from the descending trajectories that were part of the DI behind the cold front. It is also interesting to note that some of the descending trajectories had a ~ 600 hPa pressure change, which can induce localized extreme conditions that may be a crucial mesoscale features effecting the spread of the wildfires. Overall, although there was a strong positive contribution of diabatic processes, the anomalies of all trajectories after the cold front were still negative (Fig. 3a).

In summary, the Lagrangian analysis demonstrated that the record-breaking heat wave temperatures were governed by all three contributions having comparable magnitudes (left half of Fig. 3b). However, the extreme cold anomaly (right half of Fig. 3b) was governed by the transport of a climatologically colder air mass (5–12 °C), with secondary contribution of an initial cold anomaly (up to 5 °C). Because the contribution of diabatic processes is positive (heating), it counteracted the two negative anomalies, reducing the magnitude of the extreme cold anomaly, which would have been even more extreme had it been without diabatic changes along its path. Interestingly, the adiabatic heating of the air masses in the DI due to compression during their descent did not compensate enough to change the final sign of the temperature anomaly. This coherent cold anomaly brought about by descending DIs has recently been highlighted by Ilotoviz et al.[24].

The Ash Wednesday wildfires

The Ash Wednesday fires occurred in February 1983, took the lives of 75 people and consumed over 300,000 ha of rural land[7]. We

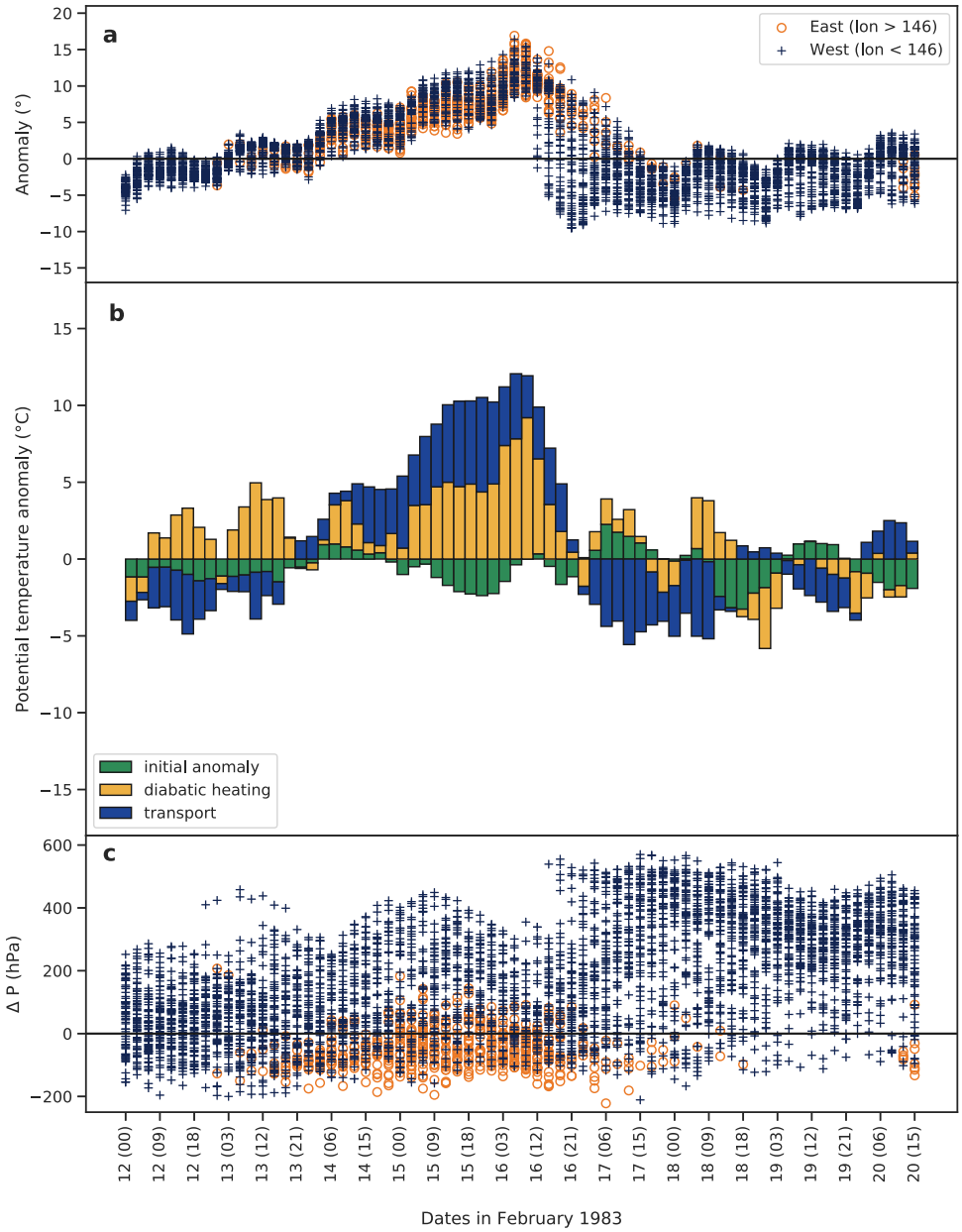

Fig. 5 Evolution of the contributing factors in the Ash Wednesday fires cold front. Trajectories presented every 3 hours between February 12–20, 1983 (hours in UTC), showing (**a**) the target θ', each point represents one trajectory. Color indicates the origin of the trajectories, east or west of 146E longitude; (**b**) the θ' decomposition; and (**c**) ΔP of each trajectory, colors as in (**a**).

performed a similar analysis of back trajectories to identify the origin of the anomalies reaching the area and contrast them with those of the Black Saturday fires. The regional synoptic situation was similar to that of the Black Saturday fires (Fig. 4), both being the typical synoptic structure characterizing extreme fire weather in Southeast Australia[11]. The associated flow patterns are similar. In the warm sector there were descending westerly trajectories and lower-tropospheric easterly trajectories. In this case, the trajectories originated closer to the continent indicating weaker winds and more local effects (Fig. 4c). In the cold sector, a coherent south and southwesterly flow was evident with and without vertical descent. A strong DI arrived from above the Antarctic coast, reaching the target area (Fig. 4d).

The results of the decomposition analysis are presented in Fig. 5. The temperature anomalies in the warm sector rose quickly and reached +16°. These anomalies were a result of descending trajectories with large ΔP as well as from easterly near-surface flows. Diabatic heating and transport of climatologically warmer air contributed to the positive anomaly in the warm sector. However, in contrast to the Black Saturday fires the initial anomaly arriving from the trajectory origin was negative, damping the warm anomaly at the target. In fact, only when the initial anomaly was minimal, on 16 February 1983, did θ' reach its peak (Fig. 5b).

The θ anomalies demonstrate the strong temperature drop across the cold front[7]. The negative anomalies were mainly a result of transport of climatologically colder air masses. Interestingly, in this case the initial anomaly and the diabatic contributions were inconsistent, changing their sign after the cold front. Both warm and cold anomalies reached the area, and the final cold anomaly, being the average of the contributions, was not as large. After the cold front, a DI formed as part of the cyclonic system shown by the very large $\triangle P$ values and large negative

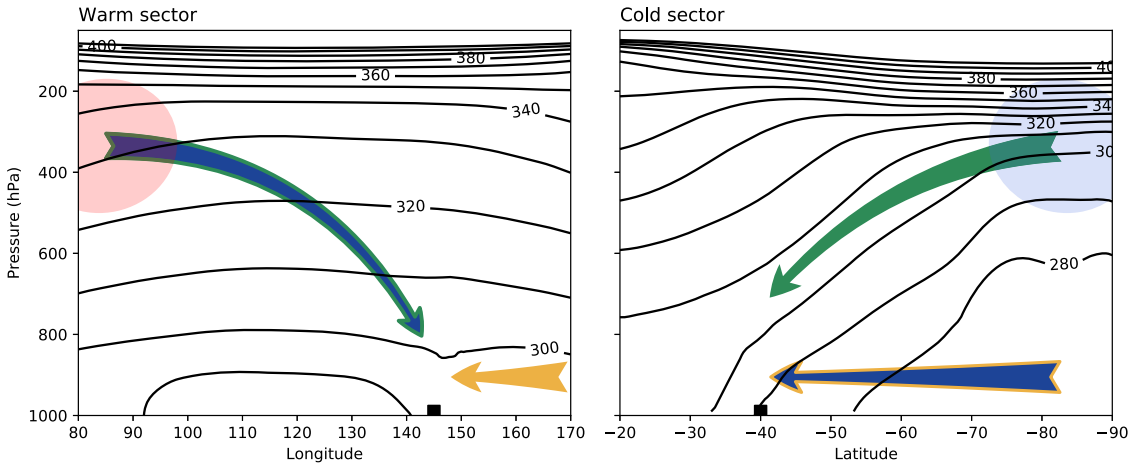

Fig. 6 Schematic diagram summarizing the air streams on both sides of the cold front. The contributing air streams to the warm anomaly before (left) and cold anomaly after (right) the passage of the cold front, using the color codes as in Figs. 3b and 5b. Background contours are the potential temperature climatology for February (K) in two cross-sections: East-West (left) and North-South (right), through145E, 30 S. The shaded circles mark initial warm and cold anomalies in red and blue, respectively. The black box roughly marks the Australian coast.

anomalies. Analysis of a single day (as in Fig. 2, not shown) showed that diabatic cooling balanced the positive transport in descending trajectories. This balance can be ascribed to radiative cooling from clouds that appeared quickly after the passage of the cold air mass[25].

In contrast to the Black Saturday event the temperature drop along the target area was much sharper (quicker), and it appears that the air flow contributions and θ' return to their pre-warm sector state much faster (right side in Fig. 5b). These differences could stem from the front propagation speed. In the case of the Ash Wednesday fires, the cold air mass passed quickly over the target area, as the front passed at a rate of ~17 m/s[25]. Following the front, sustained strong winds were evident[7], as was also seen in the elongated trajectories coming from the south west near the Antarctic coast (Fig. 4d). In the Black Saturday fires the front progressed at a rate of ~10 m/s[11], allowing the cold air mass to be sustained longer in the area.

DISCUSSION

Intense cold fronts are key to understanding the spread of the largest southeastern Australian fires. Here, the Lagrangian approach sheds light on the origins of the extreme warm and cold temperatures across the cold fronts that were key to the rapid spread of the Black Saturday and Ash Wednesday fires, two of the largest fires in the region. The decomposition of the potential temperature anomaly offers a method for isolating the diabatic changes along the trajectory, from the conserved characteristics of the air mass.

The main air streams contributing to the anomalies on both sides of the cold front are summarized in the schematic diagram in Fig. 6. In the warm sector, heat wave conditions were a result of descending airstreams from the west that advected climatologically warmer air masses together with a pre-existing positive temperature anomaly at the trajectory origin (Fig. 6a). In the Black Saturday case, this anomaly is most likely related to the tropical cyclone off the Northwestern coast of Australia (Fig. 1a) which has been shown to influence heatwaves in the Southeast Australia[14,19]. At the same time, lower-tropospheric easterlies were diabatically heated through surface heat exchange processes. As the winds shifted during the passage of the cold front, the origin of the air changed from the warmer latitudes above the Indian Ocean to colder areas along the Antarctic coast. The extreme negative anomaly at the target was a result of cross isentropic flow in the lower levels advecting colder air masses to the target area (Fig. 6b). In addition, DI flowed down the meridionally-sloping isentropes, leading to additional negative potential temperature anomalies by advecting an initial cold anomaly and further cooling diabatically along its path. In the Black Saturday fires the initial anomaly, being on average positive in the warm sector and negative in the cold sector, enhanced the target anomalies. In the Ash Wednesday fires the contribution of the initial anomalies mostly reduced the magnitude of anomalies at the surface.

The diabatic modification of the air mass along its path consisted mostly of positive contributions (heating) in the Black Saturday fires thereby enhancing the warm anomaly, and subsequently damping the cold anomaly. In the Ash Wednesday fires, diabatic heating played a key role in the warm anomaly, but was less coherent in the cold sector. It is the contrast between the two extreme anomalies across the cold front that determined the intensity of the front, a crucial component of large Australian fires[6,7].

Application of the Lagrangian approach permitted further examination of the vertical displacement of the air masses, an aspect that is integral with the examination of potential temperature by construction, compared to diagnosing the temperature itself. Referring to the conceptual picture of cyclone conveyor belts[22,26], we expect to find mostly slantwise ascending trajectories in the warm sector[27] and descending trajectories in the cold sector[21,23,28]. Since we examined anomalies close to the surface, we expected to find mostly trajectories of minimal ascent in the warm sector and descending trajectories to dominate in the cold sector. Surprisingly, we found that descending air streams, akin to the DI conceptual airstream were present on both sides of the cold front. Moreover, the descending air streams contributed to the extreme temperature drop across the cold front by first governing the maximal positive anomaly, and later contributing to the strongest cold anomaly. In the warm sector, these descending air streams are remnants of the preceding anticyclone yet they influence the local temperature anomaly close to the cold front.

Stratospheric intrusions, DIs, as well as “dry slots” seen in satellite images have been previously associated with the occurrence of large wildfires[29–31] and in the context of abrupt surface drying[32]. Also, Rossby wave breaking has previously been highlighted as a common precursor of large fires[6,14] where DIs often initiate[33]. It is important to note that in addition to the temperature anomaly, DIs are known to destabilize the boundary layer, leading to dry conditions and stronger winds at the surface which can be crucial for the spread of wildfires[23,24]. Given the important role of both the positive and negative temperature

anomalies arriving with the DIs, a more systematic, climatological analysis of this connection is needed, also in other fire-prone regions[29,34,35].

METHODS

ERA5 data

In this study we used ERA5 reanalysis data from the European Center for Medium Range Weather Forecasts (ECMWF, Hersbach et al.[36]). The 3-hourly reanalysis data are interpolated to a 0.5° horizontal grid with 137 vertical levels. Meteorological variables between 1979 and 2019 were used to calculate monthly means and potential temperature anomalies. In addition, the wind field from ERA5 is used for the calculations of back trajectories.

Trajectory calculations

We apply a Lagrangian framework to investigate the origin of the anomalies reaching the area of the Black Saturday and Ash Wednesday fires in southeast Australia, both before and after the passage of the cold front. Back trajectories were calculated using the Lagrangian analysis tool LAGRANTO v2.0[37] based on the full wind field from ERA5. Backward trajectories were initiated every 3 h for 96 h from the area between 32 S–38 S and 142E - 150E (marked in Fig. 1c). Trajectories were initiated at 100 hPa above ground level, at horizontal intervals of 80 km, with a total of 73 trajectories in each time step. In addition to the horizontal location and pressure (height) of the air mass, potential temperature, its monthly climatology and anomalies from this monthly mean are traced along each trajectory (see next subsection for definitions of climatology and anomalies).

Potential temperature anomaly decomposition

We examined the evolution of the potential temperature of the air mass to separate diabatic and adiabatic changes to this value. The anomaly of the potential temperature for each grid point in the domain was defined as $\theta' = \theta - \theta_{clim}$, where θ_{clim} is the climatology of potential temperature, calculated as the monthly average between 1979–2019. The anomaly (θ') was then traced along the trajectory by subtracting θ_{clim} from the potential temperature at each location, giving the anomaly at each 3D location of the air mass. By subtracting the anomaly at the initial back trajectory point $\theta'(t_0, x_0)$ from the anomaly at the trajectory target point in southeast Australia $\theta'(t_1, x_1)$, we can derive the components contributing to the anomaly:

$$\theta'(t_1,x_1) = \theta'(t_0,x_0) + (\theta(t_1,x_1) - \theta(t_0,x_0)) + (\theta_{clim}(t_0,x_0) - \theta_{clim}(t_1,x_1)) \quad (1b)$$

where $t_0 = t_1 - 96h$. The 96-h time frame is able to capture both diabatic and adiabatic processes in the air mass. The time frame sensitivity is discussed in the supplemental material. In case the trajectory start and ends in the same month, the climatological potential temperature θ_{clim} is dependent only on the location x. Equation (1b) describes the contributions to the potential temperature anomaly seen at the target of the trajectory, in southeast Australia. The three terms on the RHS correspond to an initial potential temperature anomaly at the origin of the air mass, diabatic heating or cooling affecting the air mass potential temperature along its trajectory, and the transport of climatologically different air to the target area. Similar methods were used to describe drivers of other extreme events such as the Greenland melts and extreme cold events[18,38,39]. Note that in this formulation the adiabatic modification of the air mass temperature by vertical motion is implicit. We complement the analysis with an examination of the vertical displacement and geographical origin of the air masses involved.

DATA AVAILABILITY

ERA5 data can be obtained from https://www.ecmwf.int/en/forecasts/dataset/ecmwf-reanalysis-v5.

CODE AVAILABILITY

LAGRANTO 2.0 is publicly available through https://iacweb.ethz.ch/staff/sprenger/lagranto/, details in ref. [37]. All other codes are available upon request.

Received: 1 January 2023; Accepted: 12 July 2023;
Published online: 03 August 2023

REFERENCES

1. Swain, D. L. A shorter, sharper rainy season amplifies California Wildfire Risk. *Geophys. Res. Lett.* **48**, 1–5 (2021).
2. Canadell, J. G. et al. Multi-decadal increase of forest burned area in Australia is linked to climate change. *Nat. Commun.* **12**, 6921 (2021).
3. Richardson, D. et al. Increased extreme fire weather occurrence in southeast Australia and related atmospheric drivers. *Weather Clim. Extrem.* **34**, 100397 (2021).
4. Pepler, A. S. & Rudeva, I. Anomalous subtropical zonal winds drive decreases in southern Australian frontal rain. *Weather Clim. Dyn.* **4**, 175–188 (2023).
5. Cai, D., Abram, N. J., Sharples, J. J. & Perkins-Kirkpatrick, S. E. Increasing intensity and frequency of cold fronts contributed to Australia's 2019-2020 Black Summer fire disaster. *Environ. Res. Lett.* **17**, 094044 (2022).
6. Reeder, M. J., Spengler, T. & Musgrave, R. Rossby waves, extreme fronts, and wildfires in southeastern Australia. *Geophys. Res. Lett.* https://doi.org/10.1002/2015GL063125 (2015).
7. Mills, G. A. A re-examination of the synoptic and mesoscale meteorology of Ash Wednesday 1983. *Aust. Meteorol. Mag.* **54**, 35–55 (2005).
8. Fiddes, S. L., Pezza, A. B. & Renwick, J. Significant extra-tropical anomalies in the lead up to the Black Saturday fires. *Int. J. Climatol.* **36**, 1011–1018 (2016).
9. Mills, G. A. Abrupt surface drying and fire weather Part 2: A preliminary synoptic climatology in the forested areas of southern Australia. *Aust. Meteorol. Mag.* **57**, 311–328 (2008).
10. Reeder, M. J. & Smith, R. K. A study of frontal dynamics with application to the Australian Summertime "Cool Change". *J. Atmos. Sci.* **44**, 687–705 (1987).
11. Engel, C. B., Lane, T. P., Reeder, M. J. & Rezny, M. The meteorology of Black Saturday. *Q. J. R. Meteorol. Soc.* **139**, 585–599 (2013).
12. Cruz, M. G. et al. Anatomy of a catastrophic wildfire: The Black Saturday Kilmore East fire in Victoria, Australia.*Ecol. Manag.* **284**, 269–285 (2012).
13. Reeder, M. J. & Smith, R. K. Australian spring and summer cold fronts. *Aust. Meteorolgical Mag.* **41**, 101–124 (1992).
14. Parker, T. J., Berry, G. J. & Reeder, M. J. The structure and evolution of heat waves in Southeastern Australia. *J. Clim.* **27**, 5768–5785 (2014).
15. Quinting, J. F. & Reeder, M. J. Southeastern Australian heat waves from a trajectory viewpoint. *Mon. Weather Rev.* **145**, 4109–4125 (2017).
16. Bieli, M., Pfahl, S. & Wernli, H. A lagrangian investigation of hot and cold temperature extremes in europe. *Q. J. R. Meteorol. Soc.* **141**, 98–108 (2015).
17. Papritz, L. & Spengler, T. A Lagrangian climatology of wintertime cold air outbreaks in the Irminger and Nordic Seas and their role in shaping air-sea heat fluxes. *J. Clim.* **30**, 2717–2737 (2017).
18. Papritz, L. Arctic lower-tropospheric warm and cold extremes: Horizontal and vertical transport, diabatic processes, and linkage to synoptic circulation features. *J. Clim.* **33**, 993–1016 (2020).
19. Parker, T. J., Berry, G. J. & Reeder, M. J. The influence of tropical cyclones on heat waves in Southeastern Australia. *Geophys. Res. Lett.* **40**, 6264–6270 (2013).
20. Bureau of Meteorology. *Special Climate Statement 73 - extreme heat and fire weather in December 2019 and January 2020. Bureau of Meteorology* http://www.bom.gov.au/climate/current/statements/ (2020).
21. Browning, K. A. The dry intrusion perspective of extra-tropical cyclone development. *Meteorol. Appl.* **4**, 317–324 (1997).
22. Wernli, H. & Davies, H. C. A Lagrangian-based analysis of extratropical cyclones. I: The method and some applications. *Q. J. R. Meteorol. Soc.* **123**, 467–489 (1997).
23. Raveh-Rubin, S. Dry intrusions: Lagrangian climatology and dynamical impact on the planetary boundary layer. *J. Clim.* **30**, 6661–6682 (2017).
24. Ilotoviz, E., Ghate, V. P. & Raveh-Rubin, S. The Impact of Slantwise Descending Dry Intrusions on the Marine Boundary Layer and Air-Sea Interface Over the ARM Eastern North Atlantic Site. *J. Geophys. Res. Atmos.* **126**, 1–24 (2021).
25. Voice, M. E. & Gauntlett, F. J. The 1983 Ash Wednesday Fires in Australia. *Mon. Weather Rev.* **112**, 584–590 (1984).

26. Carlson, T. N. Airflow through midlatitude cyclones and the comma cloud pattern. *Mon. Weather Rev.* **108**, 1498–1509 (1980).
27. Madonna, E., Wernli, H., Joos, H. & Martius, O. Warm conveyor belts in the ERA-Interim Dataset (1979-2010). Part I: Climatology and potential vorticity evolution. *J. Clim.* **27**, 3–26 (2014).
28. Catto, J. L. & Raveh-Rubin, S. Climatology and dynamics of the link between dry intrusions and cold fronts during winter. Part I: global climatology. *Clim. Dyn.* **53**, 1873–1892 (2019).
29. Langford, A. O., Pierce, R. B. & Schultz, P. J. Stratospheric intrusions, the Santa Ana winds, and wildland fires in Southern California. *Geophys. Res. Lett.* **42**, 6091–6097 (2015).
30. Schoeffler, F. J. Large Wildfire Growth Influenced by Tropospheric and Stratospheric Dry Slots in the United States. in *17th Conf. on the Middle Atmosphere* 5.1 (2013).
31. Mills, G. A. Abrupt surface drying and fire weather Part 1: Overview and case study of the South Australian fires of 11 January 2005. *Aust. Meteorol. Mag.* **57**, 299–309 (2008).
32. Mills, G. A. A re-examination of the synoptic and mesoscale meteorology of Ash Wednesday 1983. *Aust. Meteorol. Mag.* **54**, 35–55 (2005).
33. Silverman, V., Nahum, S. & Raveh-Rubin, S. Predicting origins of coherent air mass trajectories using a neural network—the case of dry intrusions. *Meteorol. Appl.* **28**, 1–18 (2021).
34. Schoeffler, F. J. *Wildland Fire Weather Associated with the 14-15 August 2015 Large Fire Growth Events in the Pacific Northwest (USA). 17th Conference on Mountain Meteorology* (2015).
35. Georgiev, C. G., Tjemkes, S. A., Karagiannidis, A., Prieto, J. & Lagouvardos, K. Observational analyses of dry intrusions and increased ozone concentrations in the environment of wildfires. *Atmosphere (Basel)* **13**, 597 (2022).
36. Hersbach, H. et al. The ERA5 global reanalysis. *Q. J. R. Meteorol. Soc.* **146**, 1999–2049 (2020).
37. Sprenger, M. & Wernli, H. The LAGRANTO Lagrangian analysis tool - Version 2.0. *Geosci. Model Dev.* **8**, 2569–2586 (2015).
38. Hermann, M., Papritz, L. & Wernli, H. A Lagrangian analysis of the dynamical and thermodynamic drivers of large-scale Greenland melt events during 1979–2017. *Weather Clim. Dyn.* **1**, 497–518 (2020).
39. Röthlisberger, M. & Papritz, L. A global quantification of the physical processes leading to near-surface cold extremes. *Geophys. Res. Lett.* **50**, 1–10 (2023).
40. Hoskins, B. A potential vorticity view of synoptic development. *Meteorol. Appl.* **4**, S1350482797000716 (1997).

ACKNOWLEDGEMENTS

We thank Lukas Papritz (ETH Zurich) for suggesting the temperature decomposition following a preliminary analysis. We are grateful to Norman Sperber for his editing and comments. We thank all group members (Weizmann Institute of Science) for their useful feedback and discussions. This research was partially supported by the Helen Kimmel center for Planetary Science at the Weizmann Institute of Science, and by a research grant from the Maggie Kaplan Research Fund.

AUTHOR CONTRIBUTIONS

Conceptualization, investigation, review writing and editing: L.M-R. and S.R-R. Writing original draft, analysis and visualization: L.M-R. Project administration and supervision: S.R-R.

COMPETING INTERESTS

The authors declare no competing interests.

ADDITIONAL INFORMATION

Supplementary information The online version contains supplementary material available at https://doi.org/10.1038/s41612-023-00425-z.

Correspondence and requests for materials should be addressed to Leehi Magaritz-Ronen.

Reprints and permission information is available at http://www.nature.com/reprints

Publisher's note Springer Nature remains neutral with regard to jurisdictional claims in published maps and institutional affiliations.